Hindawi
Geofluids
Volume 2020, Article ID 4918087, 10 pages
https://doi.org/10.1155/2020/4918087

Research Article

Hydraulic Fracturing Behavior in Shale with Water and Supercritical CO_2 under Triaxial Compression

Jianming He,[1,2,3] **Yixiang Zhang**,[1,2,3] **Chao Yin**,[1,2,3] **and Xiao Li**[1,2,3]

[1]*Key Laboratory of Shale Gas and Geoengineering, Institute of Geology and Geophysics, Chinese Academy of Sciences, Beijing 100029, China*
[2]*Innovation Academy for Earth Science, Chinese Academy of Sciences, Beijing 100029, China*
[3]*University of Chinese Academy of Sciences, Beijing 100049, China*

Correspondence should be addressed to Jianming He; hjm@mail.iggcas.ac.cn and Yixiang Zhang; zhangyixiang@mail.iggcas.ac.cn

Received 6 August 2019; Revised 24 December 2019; Accepted 21 January 2020; Published 18 March 2020

Guest Editor: Paolo Dabove

Comparing to the water fracturing fluid regularly used in the hydraulic fracturing operation, supercritical CO_2 (SC-CO_2) as a promising nonaqueous fracturing fluid has the great potential for the improvement of production and protection of shale reservoir. This paper presents an experimental study of the mechanical response and fracture propagation of shale fractured using water and SC-CO_2 under the different stress status and injection rate. According to the experimental results, SC-CO_2 fracturing is more time-consuming due to its compressibility which takes about 20 times more time than hydraulic fracturing using water under the same preset conditions. The breakdown pressure of shale can be affected by not only the anisotropy of itself but also the external factors like injection rate and deviator stress. Similar tendency of the breakdown pressure with the variation of bedding orientation can be observed in both of the fracturing using water and SC-CO_2. However, all of the shale specimens fractured using SC-CO_2 show smaller breakdown pressure if compared with the shale specimens fractured using water. According to the results of fracture width evolution monitored by circumference during the fracturing, the fracture propping and proper size of the proppant are really important for the hydraulic fracturing.

1. Introduction

Shale is composed of fine debris, clay, and organic matter (the diameter is less than 0.0039 mm) with extremely low permeability of about $10e^{-3} - 10e^{-6}$ mD [1, 2]. Hydraulic fracturing is a major technology used for the commercial development of shale gas which can significantly enhance the permeability and improve the production capacity because of large surface contact area formed between the fractures and reservoir [3–5].

Currently, water is the only fracturing fluid regularly used in the commercial shale gas development due to its low cost, availability, and its suitability for fracturing [6]. However, plenty of problems or concerns are brought by the fracturing fluid of water such as water shortages [7] and pollution of the flow-back water [8]. More importantly, shale will expand and induce a considerable strength reduction due to rich clay minerals in the presence of water [9, 10]. Consequently, it is necessary to reduce or even eliminate water requirements in hydraulic fracturing which stimulates the exploration into the use of nonaqueous fracturing fluids. Supercritical CO_2 is a notable nonaqueous fracturing fluid currently under consideration due to its particular characteristics. When temperature and pressure, respectively, exceed 31.10°C and 7.38 MPa, CO_2 is in the supercritical state. It has traits of small intermolecular forces, zero surface tension, and strong mobility. Supercritical CO_2 offers several significant advantages over water, including the water-sensitive mineral protection [10, 11], high penetration rate in the shale formation and effective gas transportation from fractures with poor connectivity [12, 13], enhanced desorption of methane (CH_4) from organics present in shale, and fast and complete flow back [14–17]. In addition, large volumes of CO_2 used for shale gas production can be stored in the deep formation which is a major option to solve the issue of greenhouse gas emission as well [18].

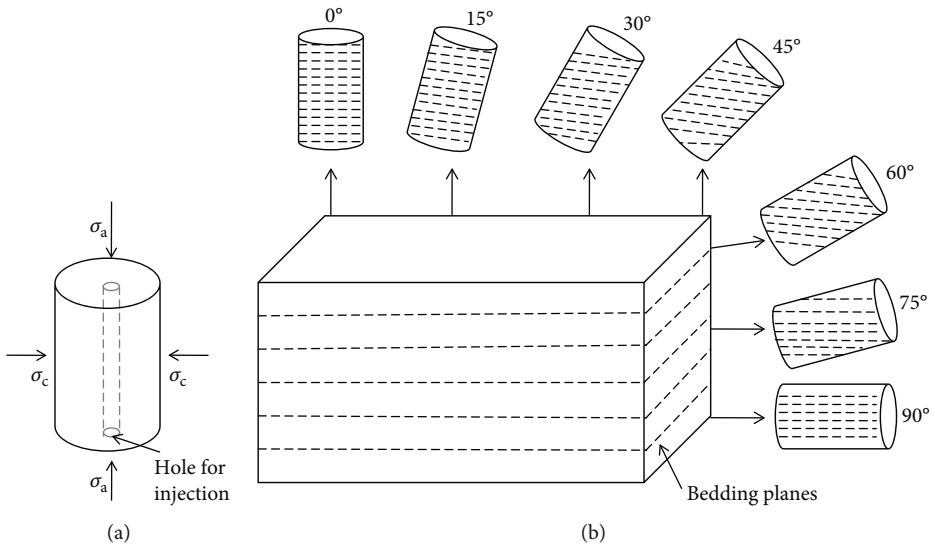

Figure 1: Diagram of (a) sample with injection hole and (b) sample with different bedding orientations.

Some researchers have compared the experimental results of hydraulic fracturing using water and SC-CO_2, especially the influence of fracturing fluid viscosity. Ishida et al. [19, 20] found that CO_2 with low viscosity tends to generate cracks extending more three-dimensionally with a larger fractal dimension. Inui et al. [21] found that low-viscosity fluid, such as SC-CO_2, could induce shear dominant fracture, while high-viscosity fluid could induce tensile dominant fracture. Chen et al. [22] observed the induced fractures of granite induced by SC-CO_2, water, and viscous oil. The results showed that the most branches were induced by SC-CO_2 than the other fracturing fluids. Zhou et al. [23] used numerical simulations to investigate the influence of fluid viscosity and compressibility to the fracturing. The results indicated that thin fluid, such as CO_2, would induce thinner and shorter fractures than water. Previous studies indicated that the natural fractures will affect the propagation of hydraulic fractures. The studies by Fan and Zhang [24] and Cheng et al. [25] indicated that both geological and engineering parameters determine whether hydraulic fractures cross the natural fractures. Zhang et al. [26] analyzed the different fracture geometry features induced by water and SC/L-CO_2 on cubic shale specimens. Zhou et al. [27] indicated that the expansion and thermal stresses due to SC-CO_2 phase change can extend the fractures.

Shale is a type of anisotropic rock with the well-developed sedimentary structures, especially the bedding planes with different orientation in the reservoir [28–31]. It is critical to study the mechanical response and fracture propagation of shale in hydraulic fracturing using water and SC-CO_2 considering its anisotropy. In this study, hydraulic fracturing experiments under triaxial compression were carried out using water and SC-CO_2 on shale specimens with varied bedding plane angles to study the characteristics of fracturing process. The shale specimens with different bedding plane angles were obtained from the same shale formation, and the borehole was drilled out along the central axis of the specimens. The effects of stress status and injection rate on the mechanical response of shale during the hydraulic fracturing were discussed while the fracturing characteristics using water and SC-CO_2 were compared.

2. Experimental Methodology

2.1. Sample Preparation. Longmaxi shale formation of the Sichuan Basin in southern China was identified as one of the areas with the greatest potential in shale gas development [2]. The rock samples used for this laboratory experiment were taken from the outcrops of Silurian Longmaxi shale formation in Chongqing, China. The shale samples contain deep black carbonaceous shale with partly visible pyrite and calcite minerals. Cubic shale blocks with a size of 300 mm $\times$ 300 mm $\times$ 300 mm were obtained from the field, and then, the shale cores were drilled from the blocks in order to minimize the weathering during the transportation process as much as possible. The cylindrical specimen with a dimension of 100 mm in height and 50 mm in diameter was used in experiment. Both end sides of the cylindrical specimen were cut to flat and paralleled to each other. It was easy to determine the intersection angles between the drilling direction and the bedding plane, as the sedimentary planes were clearly visible on the surface of the blocks. The bedding plane angles were varied from 0° to 90° at the interval of 15° (0°, 15°, 30°, 45°, 60°, 75°, and 90°) as shown in Figure 1(b). A borehole with 8 mm in diameter and 100 mm in length was drilled at the central position along the coring direction for the injection of the fracturing fluid as shown in Figure 1(a). The drilled samples without obvious visible cracks on the surface were used to perform the fracturing experiment in this study.

2.2. Experimental System. All of the experiments of hydraulic fracturing in this paper were completed on the triaxial rock testing system accompanied with the injection system of fracturing fluid. The triaxial loading system allows for the triaxial loading of rock specimens along with the

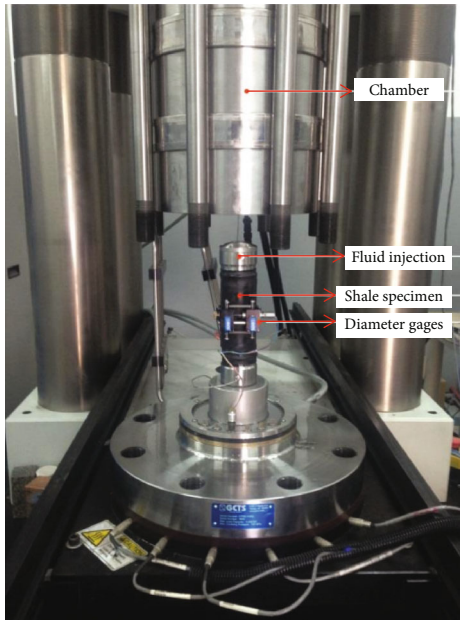

Figure 2: Shale specimen installed in the triaxial compression chamber.

simultaneous injection of fracturing fluid. Figure 2 shows the shale specimen installed in the triaxial compression chamber. Two metal blocks were glued on the shale specimens by epoxy to separate the fracturing fluid from the hydraulic oil for confining pressure. One of the metal blocks had the channel for fracturing fluid entering into the borehole. In addition, the circumferential extensometer was applied around the specimen to measure the radial strain in the process of experiment. Figure 3 shows the schematic diagram of the SC-CO_2 fracturing system. Compared with the room temperature of hydraulic fracturing using water, liquid CO_2 discharged from the cylinder was heated and controlled at 45°C after pressurization by ISCO pump to guarantee the super critical state of CO_2. A detailed discussion about SC-CO_2 fracturing system was reported by Zhang et al. (2019).

2.3. Testing Procedures. The injection rate of the fracturing fluid in the fracturing experiment was set as 0.2 or 0.3 ml/s. The confining pressure was set as 20 MPa, and the axial stress was set as 25, 30, and 35 MPa, respectively, to achieve the different deviator stresses. Step 1 was to set the stress state of the shale specimen to the target value. The rate of the confining pressure was 0.1 MPa/s while the increasing rate of axial stress was 0.2 MPa/s to achieve the target value. Thereafter, the stress status was servo controlled during the whole process of hydraulic fracturing. The next step was injecting the fracturing fluid at a preset rate into the specimen through the drilling hole. Finally, to reach an equilibrium state in the experimental system, the constant injection would last 1 more minute after the specimen fractured. The data of the axial stress, confining pressure, radial deformation, and pump pressure were recorded during the process of fracturing experiment.

To understand the effects of different fracturing fluid on the shale, the specimens were grouped into two sets for hydraulic fracturing using water and SC-CO_2, respectively. Seven different bedding plane angles (0°, 15°, 30°, 45°, 60°, 75°, and 90°) of the shale were considered in each set of specimens.

3. Results and Discussion

Experiment results can be used for understanding the fracturing process and its mechanism, especially the difference between the water fracturing and SC-CO_2 fracturing. Table 1 shows the preset conditions and breakdown pressure (peak value of pump pressure) of the different shale specimens with varied bedding plane angles. In this section, the pump pressure development and breakdown pressure variation of sample with different bedding directions are shown. The influence of deviator stress on the shale breakdown pressure is analyzed. In addition, shale fracture propagation and development of the fracture width are discussed.

3.1. Evolution of the Pump Pressure. The constant injection rate (0.3 ml/s) of water and SC-CO_2 was applied into the borehole for the fracturing of specimen under the preset triaxial stress conditions (axial stress $\sigma_a = 25$ MPa, confining pressure $\sigma_c = 20$ MPa). Figure 4 shows some typical pump pressure development for specimens with different bedding plane angles (0°, 30°, 60°, and 90°). The pump pressure increases with the injection of fracturing fluid until it peaks at the breakdown pressure, and the specimen fracturing occurs instantaneously. After that, the pump pressure dropped to a value equivalent to the confining pressure in general, which can be attributed to the connection between the fracturing fluid and confining oil in the compression chamber. It indicated that the equilibrium state between the pump pressure and confining pressure had been reached in the triaxial rock testing system.

The pressure curves of SC-CO_2 fracturing (Figure 4) show that the initial pressure is approximate 6 MPa when the liquid CO_2 is injected into the borehole. With the constant injection of the SC-CO_2, the pump pressures increase with a relatively low increase rate due to the volume compressibility of CO_2. The increase rate of CO_2 pressure increases gradually even the injection rate keeps constant, and its amplitude increased obviously before peaking at the breakdown pressure. Compared with the SC-CO_2 fracturing, the pump pressure of water fracturing only shows a little increase during the initial pressurization stage and it increases sharply at a much higher rate before the peak value breached. Therefore, hydraulic fracturing using SC-CO_2 is more time-consuming than the fracturing using water under the same experimental conditions. Table 2 shows the comparison of exact time taken for pump pressure development of fracturing using water and SC-CO_2. In general, SC-CO_2 fracturing takes about 20 times more time than water fracturing under the same experimental conditions.

3.2. Variation of the Breakdown Pressure. Shale reveals strong anisotropy in the failure strength under triaxial compression

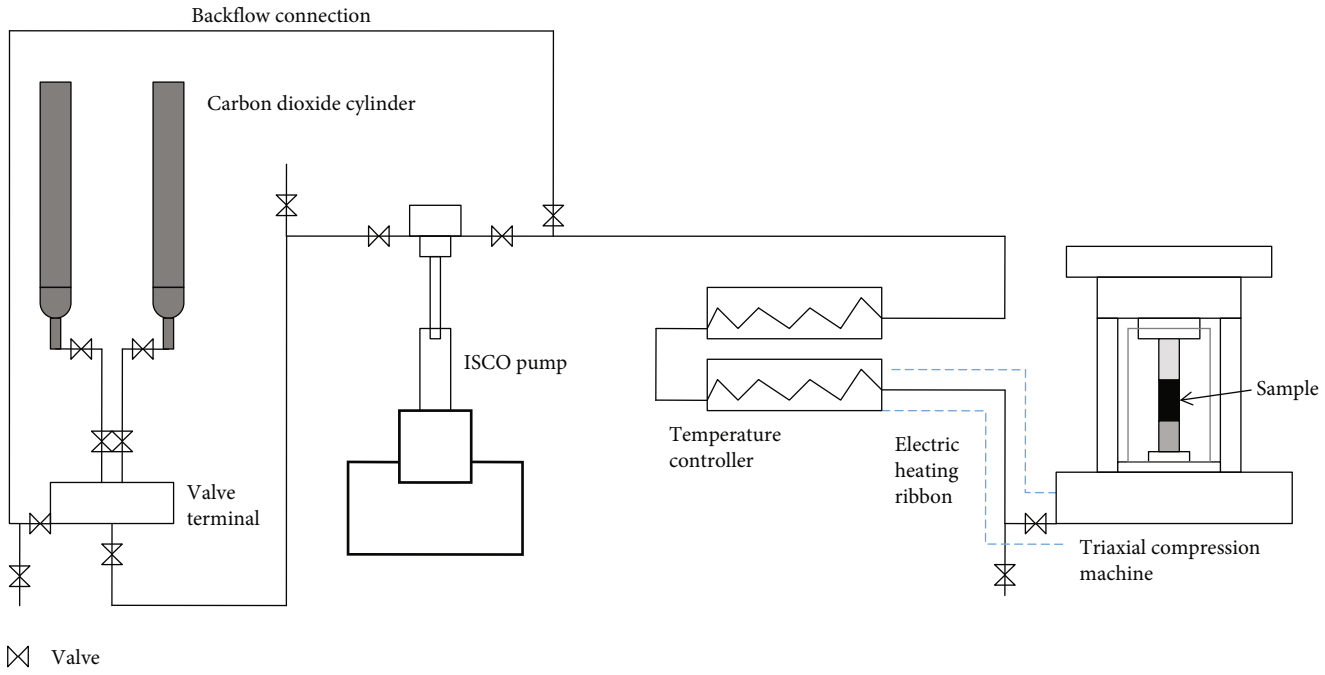

Figure 3: Schematic of SC-CO_2 fracturing system.

and Brazilian test conditions [32–34], as does in the breakdown pressure of hydraulic fracturing. The variations of breakdown pressure in hydraulic fracturing using water and SC-CO_2 versus bedding plane angle are shown in Figure 5, respectively. Breakdown pressure of the specimen with the bedding plane angle of 0° shows the highest value, and the specimen with the bedding plane angle of 90° shows the minimum value under the same experimental conditions, regardless of the fracturing fluid being water or SC-CO_2. The values of breakdown pressure of the rest of the specimens with different bedding plane angles (15°, 30°, 45°, 60°, and 75°) occur to fluctuate in a certain range depending on the failure pattern. When the sample is fractured along the bedding plane, it shows the relatively low breakdown pressure. In contrast, the samples have high breakdown pressures with failure patterns across the bedding plane. It also indicates that the breakdown pressure of the shale increases generally with the increase of injection rate of the fracturing fluid if the results of breakdown pressure in Figures 5(a) and 5(b) are compared.

The specimen fractured using SC-CO_2 shows the smaller breakdown pressure if compared with the corresponding specimen fractured using water. Table 3 shows the breakdown pressure variation of the specimens with bedding plane angle of 0° and 90° under the injection rate of 0.2 ml/s and 0.3 ml/s, respectively. The reduction proportion of breakdown pressure using water is higher than the reduction proportion of breakdown pressure using SC-CO_2 regardless of the injection rate. Therefore, the anisotropy in breakdown pressure of shale under SC-CO_2 fracturing is weaker than that under water fracturing. Furthermore, the higher injection rate of 0.3 ml/s can induce a bigger gap (from 27.06% to 39.68%) between the breakdown pressures of the fracturing using water and SC-CO_2 if compared with the lower injection rate of 0.2 ml/s (from 23.25% to 28.26%).

3.3. Effects of Deviator Stress on the Breakdown Pressure. The shale reservoir has a large depth which causes the in situ stress state to be close to the hydrostatic state, which can attribute to an insignificant deviator stress in the reservoir (Lin et al., 2018). In order to study the effects of this deviator stress on the fracturing, the confining stress of the specimens was set as 20 MPa and the axial stress was set as 25, 30, and 35 MPa, respectively. The injection rate was kept constant as 0.3 ml/s in the experiment for the comparison. The experimental results of the specimens with bedding plane angle of 0° and 90° fractured using water and SC-CO_2 under different deviator stress are shown in Figure 6.

The relationships between the deviator stress and breakdown pressure of the fracturing are shown in Figure 6. It indicates that the breakdown pressure decreases with the increase of deviator stress in the fracturing using water or SC-CO_2. It is consistent with the elasticity theory to calculate the breakdown pressure as follows [35, 36]:

$$P_b = 3\sigma_{min} - \sigma_{max} + \sigma_T, \quad (1)$$

where $_{\sigma min, \sigma max}$ represent the minimum and the maximum value in situ stress, respectively, and σ_T represents the tensile failure stress of the rock. Equation (1) shows that stress condition and tensile strength influence the breakdown pressure of rock regardless of the fracturing fluid and the higher deviator stress ($\sigma_{max} - \sigma_{min}$) can result in a lower breakdown pressure value. The specific values of the relationship are shown in Table 4. It indicates that the breakdown pressure of shale decreases by around 20% as the deviator stress

Table 1: Summary of the fracturing experiments results.

No.	Bedding plane angle	Fracturing fluid	σ_a (MPa)	σ_c (MPa)	q (ml/s)	P_b (MPa)
W1	0°	Water	25	20	0.3	70.37
W2	15°	Water	25	20	0.3	59.78
W3	30°	Water	25	20	0.3	51.77
W4	45°	Water	25	20	0.3	53.09
W5	60°	Water	25	20	0.3	59.52
W6	75°	Water	25	20	0.3	50.13
W7	90°	Water	25	20	0.3	42.45
W8	0°	Water	30	20	0.3	61.89
W9	0°	Water	35	20	0.3	57.02
W10	90°	Water	30	20	0.3	38.91
W11	90°	Water	35	20	0.3	34.53
W12	0°	Water	25	20	0.2	54.56
W13	15°	Water	25	20	0.2	44.21
W14	30°	Water	25	20	0.2	42.29
W15	45°	Water	25	20	0.2	49.86
W16	60°	Water	25	20	0.2	46.82
W17	75°	Water	25	20	0.2	43.02
W18	90°	Water	25	20	0.2	39.14
S1	0°	SC-CO_2	25	20	0.3	52.15
S2	15°	SC-CO_2	25	20	0.3	41.81
S3	30°	SC-CO_2	25	20	0.3	42.91
S4	45°	SC-CO_2	25	20	0.3	39.94
S5	60°	SC-CO_2	25	20	0.3	44.46
S6	75°	SC-CO_2	25	20	0.3	45.75
S7	90°	SC-CO_2	25	20	0.3	38.04
S8	0°	SC-CO_2	30	20	0.3	43.20
S9	0°	SC-CO_2	35	20	0.3	41.31
S10	90°	SC-CO_2	30	20	0.3	30.08
S11	90°	SC-CO_2	35	20	0.3	28.88
S12	0°	SC-CO_2	25	20	0.2	40.51
S13	15°	SC-CO_2	25	20	0.2	36.38
S14	30°	SC-CO_2	25	20	0.2	34.42
S15	45°	SC-CO_2	25	20	0.2	35.89
S16	60°	SC-CO_2	25	20	0.2	32.31
S17	75°	SC-CO_2	25	20	0.2	34.49
S18	90°	SC-CO_2	25	20	0.2	31.09

Note: σ_a denotes axial stress; σ_c denotes confining pressure; q denotes injection rate; P_b denotes breakdown pressure which is the pressure value of fracturing fluid when the specimen is fractured.

increased from 5 MPa to 15 MPa. In addition, the reduction proportion of the breakdown pressure in SC-CO_2 fracturing is slightly higher than that of hydraulic fracturing using water.

3.4. Fracture Propagation. The fracture always propagates along mechanically favorable direction in the process of hydraulic fracturing. When the fracture encounters the preexisting plane of weakness in shale, the fracture propagation would be complicated and different patterns of the fracture

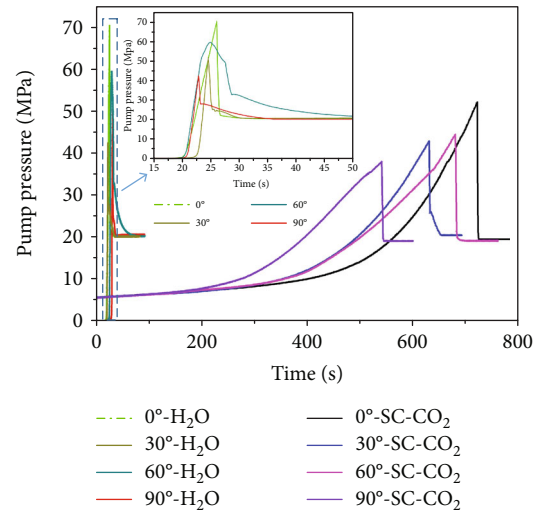

Figure 4: Typical pump pressure curves of shale fractured using water and SC-CO_2.

Table 2: Time comparison of pump pressure to peak using water and SC-CO_2.

No.	Bedding plane angle	Fracturing fluid	Injection rate (ml/s)	Time (s)	Time ratio (t_s/t_w)
W1	0°	Water	0.3	26	27.73
S1	0°	SC-CO_2		721	
W3	30°	Water		25	25.20
S3	30°	SC-CO_2		630	
W5	60°	Water		25	27.16
S5	60°	SC-CO_2		679	
W7	90°	Water		23	23.48
S7	90°	SC-CO_2		540	

t_s denotes the time of SC-CO_2 pump pressure reaching peak. t_w denotes the time of water pump pressure reaching peak.

propagation could be observed depending on the fracturing fluid, preexisting planes, and in situ stress state ([37]; Lin et al., 2017).

Previous experimental study on the hydraulic fractures demonstrated that simple and symmetrical fractures were generated around the injection hole in relatively homogeneous rocks [38]. In this study, the anisotropy of the shale caused by the variation of bedding orientation could make the propagation pattern of hydraulic fracture more complex. Figure 7 shows the morphology of main fractures formed in shale specimens after the fracturing experiment, in which different patterns of fracture propagation with complex morphology can be observed. Three typical propagation patterns can be found according to the relative orientation of hydraulic fracture with respect to the bedding plane, which include propagating across, propagating along, and being arrested.

As the case of water fracturing shown in Figure 7(a), the fracture just propagate along the bedding plane in the specimen with bedding plane angle of 45° and 90°. The fractures of

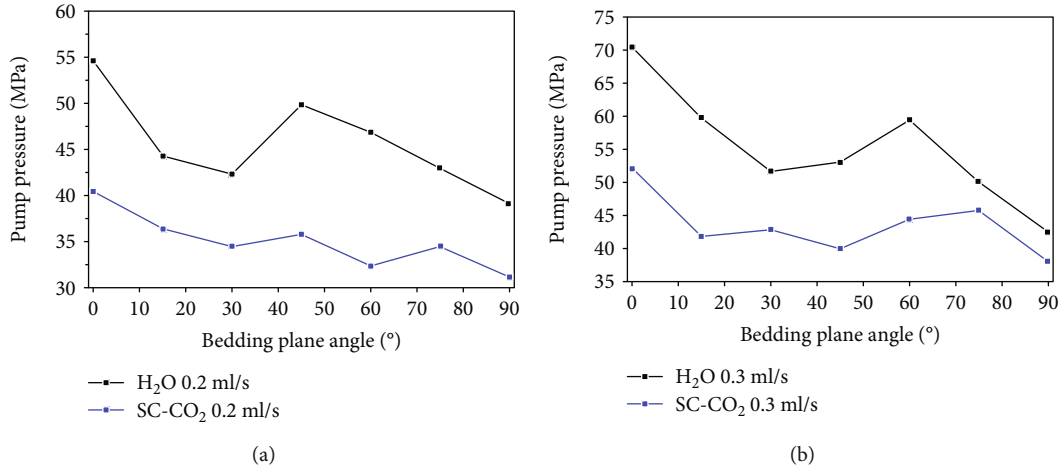

Figure 5: Variation of the breakdown pressure of fracturing using water and SC-CO_2 with the injection rate of (a) 0.2 ml/s and (b) 0.3 ml/s.

Table 3: Comparison of shale breakdown pressure variation.

No.	Bedding plane angle	Fracturing fluid	Injection rate (ml/s)	Breakdown pressure (MPa)	Reduction proportion $(((P_0 - P_{90})/P_0) \times 100\%)$
W12	0°	Water	0.2	54.56	28%
W18	90°			39.14	
S12	0°	SC-CO_2		40.51	23%
S18	90°			31.09	
W1	0°	Water	0.3	70.37	40%
W7	90°			42.45	
S1	0°	SC-CO_2		52.15	27%
S7	90°			38.04	

P_0 denotes the breakdown pressure of shale with a bedding plane angle of 0°. P_{90} denotes the breakdown pressure of shale with a bedding plane angle of 90°.

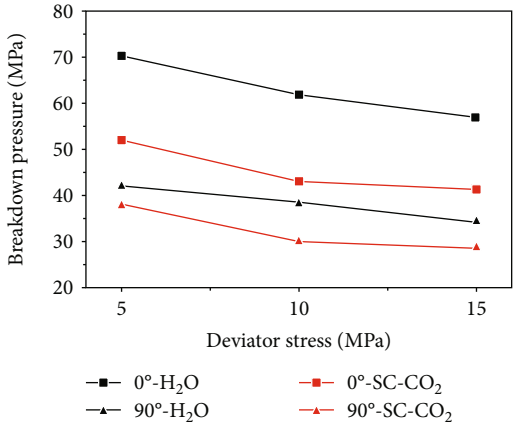

Figure 6: Influence of deviator stress on breakdown pressure with bedding plane angles 0° and 90°.

the specimens with bedding plane angle of 30° and 60° propagate across the bedding plane initially before being arrested. Both of the propagating across and propagating along the bedding plane occur in the specimens with bedding plane angle of 0°, in which the fracture can cut across the bedding plane before opening it. Comparing with the fracture formed by water fracturing, the fractures formed by SC-CO_2 fracturing can be more likely to have steep dips as shown in Figure 7(b). Most of the specimens using SC-CO_2 have fracture propagations across the bedding planes. Influenced by the bedding plane, local fractures also happen to deflect during the fracture propagation. The specimen with bedding plane angle of 45° shows the fracture propagation across the bedding plane initially before being arrested. According to the results of shale breakdown pressures, the hydraulic fracture propagation patterns have an obvious effect on the breakdown pressures with higher values across the bedding planes while relatively lower values along the bedding planes.

3.5. Evolution of the Fracture Width. In the fracturing experiment, the circumference of the specimen was monitored by circumferential extensometer installed in the compression chamber (Figure 8). The monitoring of circumference can reflect the evolution process of the fracture width to a large extent (Figure 9). The following equation can be used for the calculation of the width of main fracture.

$$D_f = \frac{\Delta C}{2}, \tag{2}$$

Table 4: Reduction proportion of shale breakdown pressure under different deviator stresses.

No.	Bedding plane angle	Fracturing fluid	Deviator stress (MPa)	Breakdown pressure (MPa)	Reduction proportion $(((P_5 - P_{15})/P_5) * 100\%)$
W1	0°	Water	5	70.37	19%
W9	0°		15	57.02	
W7	90°		5	42.45	19%
W11	90°		15	34.53	
S1	0°	$SC\text{-}CO_2$	5	52.15	21%
S9	0°		15	41.31	
S7	90°		5	38.04	24%
S11	90°		15	28.88	

P_5 denotes the breakdown pressure of shale under the deviator stress of 5 MPa in hydraulic fracturing using water or $SC\text{-}CO_2$. P_{15} denotes the breakdown pressure of shale under the deviator stress of 15 MPa in hydraulic fracturing using water or $SC\text{-}CO_2$.

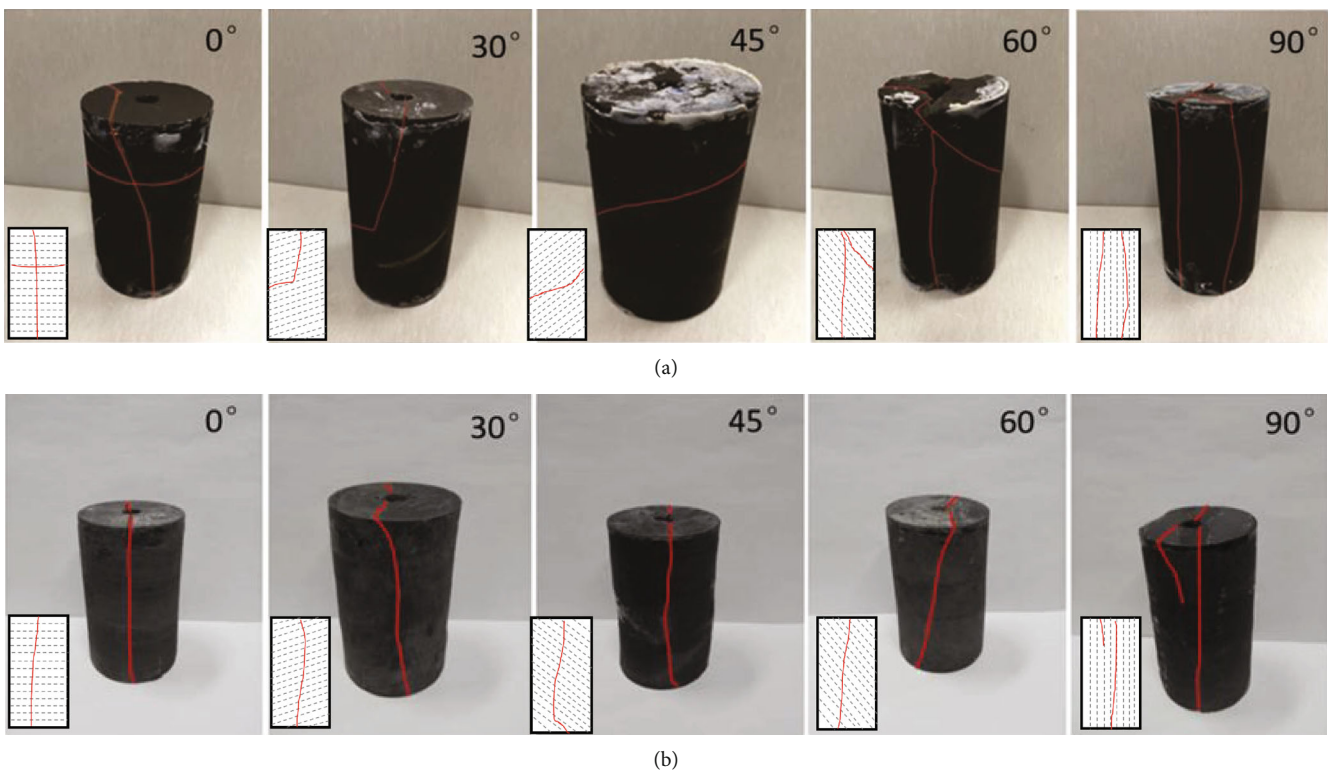

Figure 7: Macroobservation of the shale fracture morphology after fracturing. (a) Shale specimens with different bedding plane angles fractured using water. (b) Shale specimens with different bedding plane angles fractured using $SC\text{-}CO_2$. (The left-bottom diagrams show the relative orientation of hydraulic fracture with respect to the bedding plane. The red lines represent the macrofractures while the dashed lines represent the bedding planes.)

where ΔC means the variation of the circumference [38]. To improve the accuracy of fracture width calculation, the specimens with simple and symmetrical fracture morphology were selected for the study. It should be mentioned that this is an indirect method to characterize the evolution of fracture width. Table 5 shows the fracture width at different stages during the fracturing using water and $SC\text{-}CO_2$, which include maximum fracture width when the breakdown occurred (circumference from fracture initiation to the valley), opening fracture width during the equilibrium state (circumference from fracture initiation to the stable), closure of the fracture (circumference from fracture stable to the valley), and the closure proportion that the fracture closure takes in the maximum width.

Comparing the experiment results of the specimens with bedding plane angles of 0° and 90°, the fracture widths (including the maximum width and opening width), fracture closure, and closure proportion of the specimens fractured using $SC\text{-}CO_2$ are greater than the corresponding values of specimens fractured using water. The volume expansion of

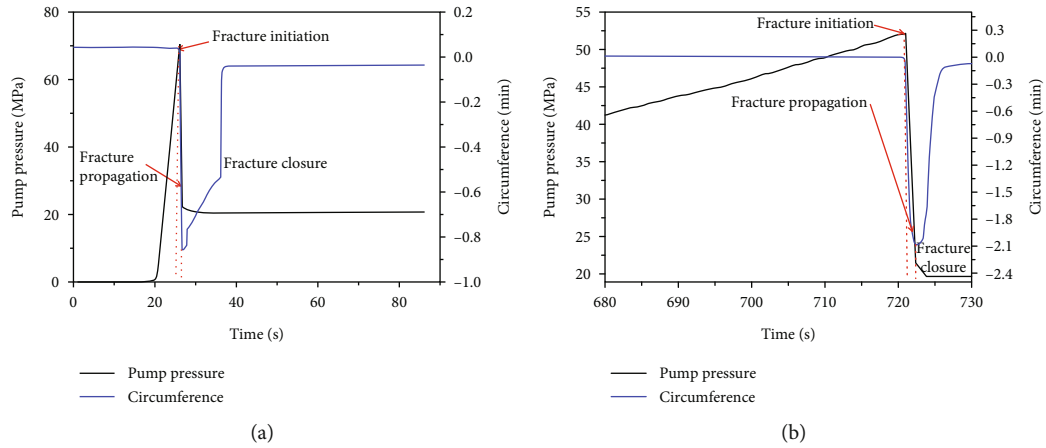

Figure 8: Curves of hydraulic fracturing using (a) water and (b) SC-CO_2 of shale with bedding plane angle of 0° under axial stress 25 MPa, confining pressure 20 MPa, and injection rate 0.3 ml/s. (The fracture width evolution was calculated. The maximum fracture width was calculated by the circumference difference from fracture initiation to the valley. The opening fracture width during the equilibrium state was by circumference difference from fracture initiation to the stable. The closure of the fracture was by circumference difference from fracture stable to the valley.)

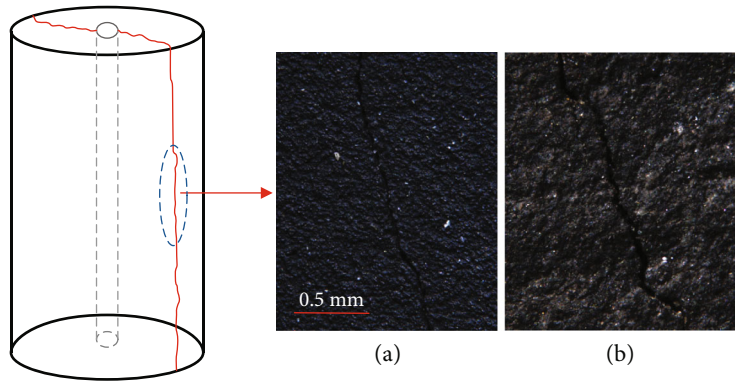

Figure 9: Microscopic images of the local cracks fractured using (a) water and (b) SC-CO_2.

Table 5: Variation of the fracture width during the hydraulic fracturing experiments.

No.	Bedding plane angle (°)	Fracturing fluid	Maximum width (mm)	Opening width (mm)	Closure (mm)	Closure proportion (closure/max) (%)
W1	0°	Water	0.428	0.019	0.409	96
S1	0°	SC-CO_2	1.054	0.039	1.015	96
W7	90°	Water	0.052	0.014	0.038	73
S7	90°	SC-CO_2	1.000	0.040	0.960	96

SC-CO_2 would be more significant after the fracture initiation occurs, which could result in the greater fracture width. In addition, the closure of fracture is considerable and the closure proportions are over 96.00% for SC-CO_2 fracturing, which is much greater than water fracturing. The fracture width of the initiation, propagation, and closure stages indicate that the fracture closure dominates the fracture evolution process. The fracture propping and proper size of the proppant are really important for the hydraulic fracturing.

4. Conclusion

The economic viability of shale reservoir development largely depends on the effective hydraulic fracture operation. The fracturing treatment using water has become a common method for the exploitation and SC-CO_2 fracturing, which can be seen as a promising method, really can bring some different effects to the shale reservoir. In this study, hydraulic fracturing experiments under triaxial compression using water and SC-CO_2 were carried out on the shale specimens

with different bedding plane angles for better understanding the different fracturing behavior. The following conclusions can be drawn:

(1) Under constant injection of the fracturing fluid, the loading rate of SC-CO_2 pressure increases gradually due to the compressibility of CO_2 while the loading rate of water pressure increases sharply before it reaches the peak value during the fracturing process. Therefore, SC-CO_2 fracturing is more time-consuming which takes about 20 times more time than hydraulic fracturing using water under the same experimental conditions

(2) Multiple external factors have influence on the breakdown pressure of shale, such as fracturing fluid and deviator stress. The shale specimens fractured using SC-CO_2 show the smaller breakdown pressure and weaker anisotropy. The breakdown pressure decreases with the increase in the deviator stress in the fracturing process, of which the reduction proportion in SC-CO_2 fracturing is slightly higher than that of water fracturing

(3) Anisotropy of the shale caused by the variation of bedding orientation can affect the fracture propagation with respect to the bedding plane, which shows three typical patterns, including propagating across, propagating along, and being arrested. The fractures formed by SC-CO_2 are more likely to propagate across the bedding plane if compared with the fractures formed by water due to its low viscosity and strong diffusibility

(4) The monitoring of pump pressure and circumference can indicate the evolution of hydraulic fractures. The fracture width in the process of SC-CO_2 fracturing shows greater value at different stages, which either does the closure between the breakdown and opening width. The fracture propping and proper size of the proppant are really important for the hydraulic fracturing

Data Availability

All data of the research results are presented in the paper.

Conflicts of Interest

The authors declare that they have no conflicts of interest.

Acknowledgments

This work was supported by the National Natural Science Foundation of China (Grant Nos. 41572310 and 41877270).

References

[1] H. Wang, G. Li, and Z. Shen, "A feasibility analysis on shale gas exploitation with supercritical carbon dioxide," *Energy Sources, Part A: Recovery, Utilization, and Environmental Effects*, vol. 34, no. 15, pp. 1426–1435, 2012.

[2] C. Zou, D. Dong, S. Wang et al., "Geological characteristics and resource potential of shale gas in China," *Petroleum Exploration and Development*, vol. 37, no. 6, pp. 641–653, 2010.

[3] B. Faraj and M. Brown, *AV Key Attributes of Canadian and US Productive Shales: Scale and Variability*, AAPG Annual Convention, New Orleans, LA, USA, 2010.

[4] G. E. King, "Thirty years of gas shale fracturing: what have we learned?," in *SPE Annual Technical Conference and Exhibition*, Florence, Italy, September 2010.

[5] M. C. Vincent, "Refracs: why do they work, and why do they fail in 100 published field studies?," in *SPE Annual Technical Conference and Exhibition*, Florence, Italy, September 2010.

[6] R. S. Middleton, J. W. Carey, R. P. Currier et al., "Shale gas and non-aqueous fracturing fluids: opportunities and challenges for supercritical CO_2," *Applied Energy*, vol. 147, no. 3, pp. 500–509, 2015.

[7] B. R. Scanlon, R. C. Reedy, and J. P. Nicot, "Comparison of water use for hydraulic fracturing for unconventional oil and gas versus conventional oil," *Environmental Science & Technology*, vol. 48, no. 20, pp. 12386–12393, 2014.

[8] R. E. Jackson, A. W. Gorody, B. Mayer, J. W. Roy, M. C. Ryan, and D. R. van Stempvoort, "Groundwater protection and unconventional gas extraction: the critical need for field-based hydrogeological research," *Ground Water*, vol. 51, no. 4, pp. 488–510, 2013.

[9] H. Emadi, M. Y. Soliman, R. Samuel, L. R. Heinze, R. B. Moghaddam, and S. Hutchison, "An experimental study of the swelling properties of unconventional shale oil rock samples using both water-based and oil-based muds," in *SPE/IADC Drilling Conference and Exhibition*, London, England, UK, March 2015.

[10] K. Makhanov, A. Habibi, H. Dehghanpour, and E. Kuru, "Liquid uptake of gas shales: a workflow to estimate water loss during shut-in periods after fracturing operations," *Journal of Unconventional Oil and Gas Resources*, vol. 7, pp. 22–32, 2014.

[11] H. Dehghanpour, H. A. Zubair, A. Chhabra, and A. Ullah, "Liquid intake of organic shales," *Energy & Fuels*, vol. 26, no. 9, pp. 5750–5758, 2012.

[12] R. Heller and M. Zoback, "Adsorption of methane and carbon dioxide on gas shale and pure mineral samples," *Journal of Unconventional Oil and Gas Resources*, vol. 8, pp. 14–24, 2014.

[13] J. W. Jung, D. N. Espinoza, and J. C. Santamarina, "Properties and phenomena relevant to CH_4-CO_2 replacement in hydrate-bearing sediments," *Journal of Geophysical Research Atmospheres*, vol. 115, no. B10, pp. 155–162, 2010.

[14] A. Abedini and F. Torabi, "On the CO_2 storage potential of cyclic CO_2 injection process for enhanced oil recovery," *Fuel*, vol. 124, pp. 14–27, 2014.

[15] K. E. Friehauf and M. M. Sharma, "Fluid selection for energized hydraulic fractures," in *SPE Annual Technical Conference and Exhibition*, New Orleans, LA, USA, October 2009.

[16] A. P. Gupta, A. Gupta, and J. Langlinais, "Feasibility of Supercritical Carbon Dioxide as a Drilling Fluid for Deep Underbalanced Drilling Operation," in *SPE Annual Technical Conference and Exhibition*, Dallas, TX, USA, October 2005.

[17] W. Yu, H. R. Lashgari, K. Wu, and K. Sepehrnoori, "CO_2 injection for enhanced oil recovery in Bakken tight oil reservoirs," *Fuel*, vol. 159, pp. 354–363, 2015.

[18] Y. Gensterblum, A. Busch, and B. M. Krooss, "Molecular concept and experimental evidence of competitive adsorption of H_2O, CO_2 and CH_4 on organic material," *Fuel*, vol. 115, pp. 581–588, 2014.

[19] T. Ishida, Q. Chen, Y. Mizuta, and J. C. Roegiers, "Influence of fluid viscosity on the hydraulic fracturing mechanism," *Journal of Energy Resources Technology*, vol. 126, no. 3, pp. 190–200, 2004.

[20] T. Ishida, K. Aoyagi, T. Niwa et al., "Acoustic emission monitoring of hydraulic fracturing laboratory experiment with supercritical and liquid CO_2," *Geophysical Research Letters*, vol. 39, no. 16, article 16309, 2012.

[21] S. Inui, T. Ishida, Y. Nagaya, Y. Nara, Y. Chen, and Q. Chen, "AE monitoring of hydraulic fracturing experiments in granite blocks using SC-CO_2, water and viscous oil," in *48th US Rock Mechanics/Geomechanics Symposium*, Minneapolis, MN, USA, June 2014.

[22] Y. Chen, Y. Nagaya, and T. Ishida, "Observations of fractures induced by hydraulic fracturing in anisotropic granite," *Rock Mechanics and Rock Engineering*, vol. 48, no. 4, pp. 1455–1461, 2015.

[23] X. Zhou and T. J. Burbey, "Fluid effect on hydraulic fracture propagation behavior: a comparison between water and supercritical CO_2-like fluid," *Geofluids*, vol. 14, no. 2, pp. 174–188, 2014.

[24] T. Fan and G. Zhang, "Laboratory investigation of hydraulic fracture networks in formations with continuous orthogonal fractures," *Energy*, vol. 74, pp. 164–173, 2014.

[25] W. Cheng, Y. Jin, and M. Chen, "Experimental study of step-displacement hydraulic fracturing on naturally fractured shale outcrops," *Journal of Geophysics and Engineering*, vol. 12, no. 4, pp. 714–723, 2015.

[26] X. Zhang, Y. Lu, J. Tang, Z. Zhou, and Y. Liao, "Experimental study on fracture initiation and propagation in shale using supercritical carbon dioxide fracturing," *Fuel*, vol. 190, pp. 370–378, 2017.

[27] D. Zhou, G. Zhang, X. Zhang et al., "Effects of super-critical CO_2 phase change on dynamic multi-fracturing process in reservoir stimulation," in *51th U.S. Rock Mechanics/Geomechanics Symposium*, San Francisco, CA, USA, June 2017.

[28] D. N. Dewhurst and A. F. Siggins, "Impact of fabric, microcracks and stress field on shale anisotropy," *Geophysical Journal of the Royal Astronomical Society*, vol. 165, no. 1, pp. 135–148, 2006.

[29] J. E. Johnston and N. I. Christensen, "Seismic anisotropy of shales," *Journal of Geophysical Research Solid Earth*, vol. 100, no. B4, pp. 5991–6003, 1995.

[30] H. Kim, J. W. Cho, I. Song, and K. B. Min, "Anisotropy of elastic moduli, p-wave velocities, and thermal conductivities of Asan gneiss, Boryeong shale, and Yeoncheon schist in Korea," *Engineering Geology*, vol. 147-148, no. 5, pp. 68–77, 2012.

[31] A. Zhubayev, M. E. Houben, D. M. J. Smeulders, and A. Barnhoorn, "Ultrasonic velocity and attenuation anisotropy of shales, Whitby, United Kingdom," *Geophysics*, vol. 81, no. 1, pp. D45–D56, 2016.

[32] Z. K. Hou, C. H. Yang, Y. T. Guo et al., "Experimental study on anisotropic properties of Longmaxi formation shale under uniaxial compression," *Rock and Soil Mechanics*, vol. 36, pp. 2541–2550, 2015.

[33] J. He and L. O. Afolagboye, "Influence of layer orientation and interlayer bonding force on the mechanical behavior of shale under Brazilian test conditions," *Acta Mechanica Sinica*, vol. 34, no. 2, pp. 349–358, 2018.

[34] Y. Chuanliang, D. Jingen, H. Lianbo et al., "Brittle failure of shale under uniaxial compression," *Arabian Journal of Geosciences*, vol. 8, no. 5, pp. 2467–2475, 2015.

[35] D. R. Schmitt and M. D. Zoback, "Poroelastic effects in the determination of the maximum horizontal principal stress in hydraulic fracturing tests–a proposed breakdown equation employing a modified effective stress relation for tensile failure," *International Journal of Rock Mechanics and Mining Sciences & Geomechanics Abstracts*, vol. 26, no. 6, pp. 499–506, 1989.

[36] S. Timoshenko and J. N. Goodier, *Theory of Elasticity*, McGraw-Hill Book Company, 2nd edition, 1951.

[37] D. Xu, R. Hu, W. Gao, and J. Xia, "Effects of laminated structure on hydraulic fracture propagation in shale," *Petroleum Exploration and Development*, vol. 42, no. 4, pp. 573–579, 2015.

[38] J. He, C. Lin, X. Li, Y. Zhang, and Y. Chen, "Initiation, propagation, closure and morphology of hydraulic fractures in sandstone cores," *Fuel*, vol. 208, pp. 65–70, 2017.